Mutual 3:1 subharmonic synchronization in a micromachined silicon disk resonator

Parsa Taheri-Tehrani, Andrea Guerrieri, Martial Defoort, Attilio Frangi, and David A. Horsley

Citation: Appl. Phys. Lett. **111**, 183505 (2017);
View online: https://doi.org/10.1063/1.4997195
View Table of Contents: http://aip.scitation.org/toc/apl/111/18
Published by the American Institute of Physics

Mutual 3:1 subharmonic synchronization in a micromachined silicon disk resonator

Parsa Taheri-Tehrani,[1,a)] Andrea Guerrieri,[2,b)] Martial Defoort,[1] Attilio Frangi,[2] and David A. Horsley[1,a)]
[1]*Department of Mechanical and Aerospace Engineering, University of California, Davis, California 95616, USA*
[2]*Department of Civil and Environmental Engineering, Politecnico di Milano, 20133 Milano, Italy*

(Received 21 July 2017; accepted 21 October 2017; published online 1 November 2017)

We demonstrate synchronization between two intrinsically coupled oscillators that are created from two distinct vibration modes of a single micromachined disk resonator. The modes have a 3:1 subharmonic frequency relationship and cubic, non-dissipative electromechanical coupling between the modes enables their two frequencies to synchronize. Our experimental implementation allows the frequency of the lower frequency oscillator to be independently controlled from that of the higher frequency oscillator, enabling study of the synchronization dynamics. We find close quantitative agreement between the experimental behavior and an analytical coupled-oscillator model as a function of the energy in the two oscillators. We demonstrate that the synchronization range increases when the lower frequency oscillator is strongly driven and when the higher frequency oscillator is weakly driven. This result suggests that synchronization can be applied to the frequency-selective detection of weak signals and other mechanical signal processing functions. *Published by AIP Publishing.* https://doi.org/10.1063/1.4997195

Phase synchronization is a well-known phenomenon used in several scientific fields.[1–4] The first documented reports of the synchronization phenomenon date back to the seventeenth century when Huygens[5] observed synchronization between two self-sustained, almost identical, ship navigation clocks whose motion was coupled through a common suspension beam. The most basic form of synchronization is based on unidirectional coupling and is also known as injection locking:[6–8] The frequency of a first oscillator, f_1, is caused to synchronize (lock) to the frequency of a second reference oscillator, f_2, by injecting the second oscillator's output into the first oscillator. The range of frequencies over which this locking can occur is called the synchronization range, and this range increases with the amplitude of the reference oscillator and with certain types of amplitude-dependent nonlinearities in the first oscillator.[9,10] Synchronization can also occur when the two frequencies have a harmonic relationship, $f_2 = nf_1$, where n is an integer, a phenomenon known as subharmonic synchronization.[11–14] Distinct from injection locking, mutual synchronization and mutual subharmonic synchronization occur when there is mutual, bidirectional coupling between the two oscillators.[10,15–20] In oscillators based on micro- and nano-electromechanical systems (MEMS and NEMS) resonators, mutual synchronization is of interest because, assuming constant strain-energy density, oscillator phase noise increases as the physical volume of a resonator decreases. As a result, NEMS and MEMS-based oscillators tend to have greater phase noise than their macroscopic equivalents. However, it has been shown that phase noise can be reduced below the individual-resonator level by mutually synchronizing multiple resonators.[21] Synchronization in these NEMS and MEMS devices is most commonly demonstrated by coupling two different resonators either electronically[17] or mechanically via electrostatic force,[20,22] light,[23,24] or flexures.[25,26] The need to use multiple resonators in these demonstrations introduces a serious flaw in this approach, since the original goal of miniaturization is reduced size. Here, we consider a different approach that requires no additional device area: rather than synchronizing two resonators operating at the same vibration mode, we start with a single resonator and synchronize two different vibration modes which have a 3:1 subharmonic frequency relationship. To date, this approach has seen little attention, in part due to the difficulty of obtaining close 3:1 frequency-matching between the two modes. Antonio *et al.*[27] solved the frequency-matching problem by exploiting a resonator nonlinearity that results in amplitude-frequency (A-*f*) dependence—the first vibration mode's amplitude was adjusted until the desired 3:1 frequency relationship with the second mode was achieved. This solution has the disadvantage that the effect of resonator amplitude on the synchronization range cannot be studied independently since amplitude and frequency are coupled. To overcome this limitation, we study synchronization using a micromachined disk resonator (MDR) originally designed to operate as a mode-matched gyroscope.[28] Mode-shape specific frequency-tuning electrodes enable the resonant frequency of the first mode to be voltage-controlled, independent of the frequency of the second mode. This capability enables us to study the synchronization range as a function of the frequency and amplitude of the two modes. We observe that the synchronization range increases as the first mode is driven to larger amplitudes but, surprisingly, the range decreases as the amplitude of the second, higher-frequency mode is increased. This result suggests

[a)]Authors to whom correspondence should be addressed: ptaheri@ucdavis.edu and dahorsley@ucdavis.edu.
[b)]Part of this research was performed while A. Guerrieri was a visiting scholar at the Department of Mechanical and Aerospace Engineering, University of California, Davis California.

that mutual synchronization may have application to the detection of weak signals around the frequency of the second mode, as any perturbation to this mode's amplitude would result in loss of synchronization and a corresponding change in oscillation frequency.

The MDR is a 40 μm thick, 600 μm diameter, single-crystal Si (Silicon) disk that is perforated by concentric annular slots and supported by a central anchor, shown in Fig. 1(a). The fabrication process, described elsewhere,[29] uses a Si (Silicon) epitaxy reactor to vacuum seal the released resonator in an inert gas environment at a pressure of 1 Pa, a process that results in high quality factor (Q) of the resonance modes and a high degree of frequency stability, due to the cleanliness of the resonator surface. The MDR is surrounded by parallel-plate electrodes that enable electrostatic transduction and frequency tuning of the resonance modes. Two separate electrode pairs are used to drive and sense the motion of the two resonance modes. Phase-locked loops (PLLs) implemented in a digital lock-in-amplifier (LIA, Zurich Instruments HF2LI) are used to operate the two resonance modes as self-sustained oscillators (e.g., van der Pol self-sustained oscillators[30,31]) by locking the oscillation phase at -90° relative to the drive voltage.[32]

Figure 1(b) shows the measured frequency sweep of the two resonance modes of interest along with their mode shapes simulated via finite element model [(FEM), Comsol Multiphysics]. As shown in the figure, each mode shape is described by $u(\theta) = u_n \cos(n\theta + \phi)$, where u_n is the maximum radial displacement, θ is the angular coordinate, n is an integer, and ϕ is the rotation of the first anti-node relative to the electrode coordinates. Note that, while a perfect disk exhibits degenerate $\cos(n\theta)$, $\sin(n\theta)$ mode pairs, fabrication imperfections split the frequencies of these pairs such that they are separated by more than the 100 Hz measured frequency range.[28] In this letter, the first mode of interest is an $n = 3$ mode (referred to as 3θ mode) and has a resonance frequency of $f_1 = 278$ kHz and a quality factor of $Q_1 = 15\,000$. The second mode is an $n = 9$ mode (referred to as 9θ mode) with $Q_2 = 60\,000$ and was selected because it has a resonance frequency that is nearly a harmonic of the first frequency ($f_2 \approx 3\ f_1$). As a result of cubic stiffness-softening introduced by the parallel-plate electrodes,[33] the two modes exhibit Duffing nonlinear amplitude-frequency (A-f) dependence.[32,34]

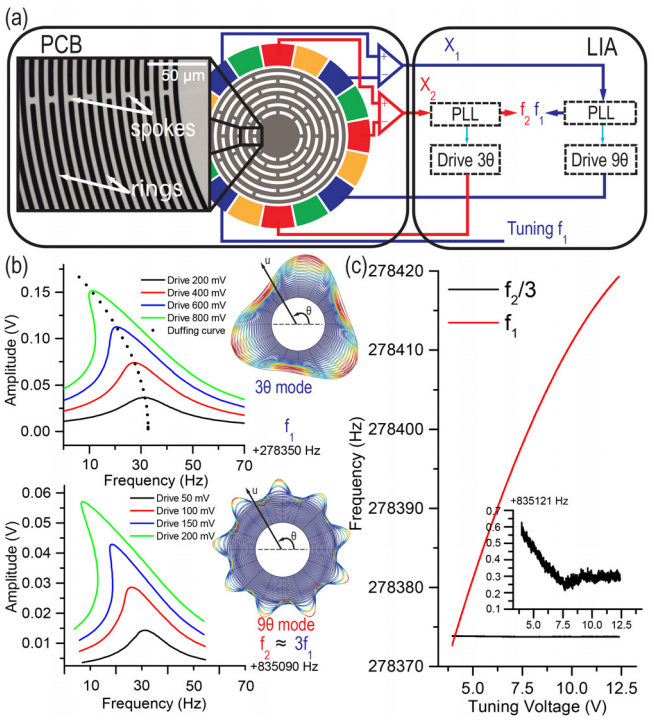

FIG. 1. (a) Microdisk resonator and experimental test setup. Two separate PLLs are used to operate the two selected modes as independent oscillators. A dc voltage applied to a tuning electrode is used to tune f_1, the frequency of the first mode. (b) Measured frequency response of the 3θ and 9θ resonance modes, and their corresponding mode shapes. The response was measured for four different input amplitudes, showing softening Duffing A-f dependence arising from electrostatic nonlinearity. (c) Frequencies f_1 (red) and f_2/3 (black) versus tuning voltage, plotted on the same scale for ease of comparison. Inset: close-up of f_2 demonstrating independence from tuning voltage.

To effectively study the synchronization range and the interactions of the two oscillators within this range, it is essential to be able to change the frequency of one oscillator independent from that of the other oscillator. Figure 1(c) presents measurements to show that the frequency of the 3θ oscillator can be controlled independently from the frequency of the 9θ oscillator using voltage applied to a tuning electrode. When the tuning voltage is increased, the voltage difference between the disk (which is biased at 16.5 V) and the tuning electrode decreases, decreasing this electrode's electrostatic stiffness and increasing f_1. The increase in frequency is quadratic because the electrostatic stiffness-constant is proportional to the square of the voltage difference.[35] The same experiment illustrates that f_2 remains unchanged as the tuning voltage is varied. This independence in tuning of the frequency allows the interaction of the two modes to be studied as f_1 is varied in the neighborhood of $f_2/3$ in the synchronized and unsynchronized states. Independent tuning is possible for two main reasons: first, the selected tuning electrode overlaps both nodes and anti-nodes of the 9θ mode shape, resulting in weak coupling to this mode;[35] and second, the stiffness of the 9θ mode is much higher than that of the 3θ mode, and is much greater than the electrostatic stiffness of the tuning electrode.

Figure 2 illustrates the measured synchronization between the 3θ and 9θ modes as the 3θ mode's frequency is tuned over a 1 V range. In these experiments, the 9θ mode (at frequency f_2) is weakly excited with 35 mV and the 3θ mode (at frequency f_1) is strongly driven at two different amplitudes to demonstrate the dependence of the synchronization range on the oscillator's amplitude. As the tuning voltage is increased, f_1 increases and approaches $f_2/3$ from below (upwards frequency sweep). As f_1 approaches $f_2/3$, the amplitude of quasi-periodic oscillation with a frequency of $f_1 - f_2/3$ increases until the two frequencies collapse on each other. At this stage, the 9θ mode's oscillation frequency, despite being independent from the tuning voltage, will follow $3f_1$ due to synchronization. As the tuning voltage is increased further, the modes eventually exit the synchronized state and quasi-periodic oscillations in both modes reappear. The same experiment was conducted by decreasing the tuning voltage such that f_1 approaches $f_2/3$ from above (downwards frequency sweep). A similar behavior is observed in this experiment as well, with a difference that, when the 3θ

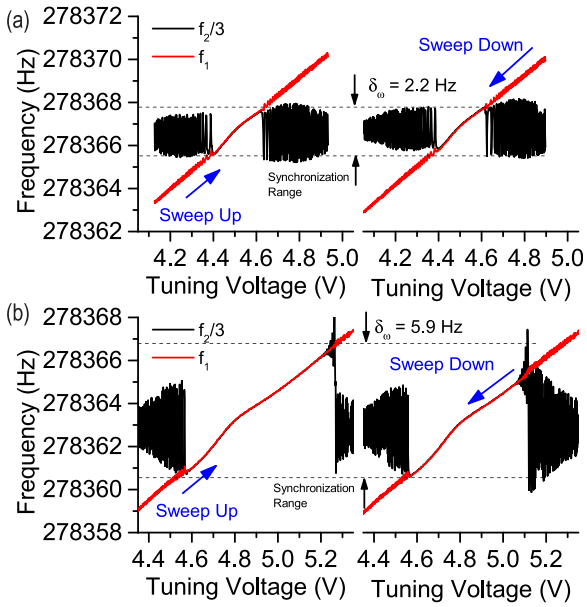

FIG. 2. Synchronization range measured for upwards and downwards frequency sweeps at f_2: 35 mV and two different amplitudes for f_1: (a) 650 mV drive and (b) 750 mV drive. When the f_1 oscillator's amplitude is increased, the downwards sweep shows a smaller synchronization range than the upwards sweep.

mode is driven at a larger amplitude, the synchronization range increases but the range when sweeping down is smaller than when sweeping up. An asymmetric synchronization range is observed when the resonance modes have nonlinearities and this asymmetry has been previously reported in injection-locked oscillators[9,10] and mutual synchronization.[20]

To study the theoretical behavior of the coupled oscillators, we introduce a model which explains this behavior. The two resonance modes are coupled through linear and nonlinear electromechanical stiffness terms.[36] This coupling is essential to make subharmonic synchronization possible. The model includes cubic coupling terms because first, as shown in Fig. 1, both modes exhibit Duffing nonlinearities and second, in a first-order approximation, only cubic coupling nonlinearities create internal resonance between the two resonance modes.[37,38] Simplified two degree-of-freedom (DOF) equations of motion can model the behavior of the resonance modes in the synchronized state

$$\begin{aligned}\ddot{x}_1 + \Delta\omega_1\dot{x}_1 + \omega_1^2 x_1 &= k_1x_1^3 + k_2x_1^2x_2 + k_3x_1x_2^2 + k_4x_2^3 + \lambda_1,\\ \ddot{x}_2 + \Delta\omega_2\dot{x}_2 + \omega_2^2 x_2 &= k_5x_1^3 + k_6x_1^2x_2 + k_7x_1x_2^2 + k_8x_2^3 + \lambda_2.\end{aligned} \tag{1}$$

In these equations, x_1 and x_2 are the modal amplitudes of the 3θ and 9θ resonance modes with resonant frequencies $\omega_1 = 2\pi f_1$ and $\omega_2 = 2\pi f_2$, respectively. $\Delta\omega_1 = \omega_1/Q_1$ and $\Delta\omega_2 = \omega_2/Q_2$ are the full width at half maximum (FWHM) bandwidths of the two modes. λ_1 and λ_2 are external forces applied to the modes. The stiffness terms k_1 and k_8 are cubic terms that result in Duffing nonlinearity in single DOF resonators, while k_2 through k_7 represent the nonlinear coupling between the two modes. Using a perturbation and multiple time-scales method with $x_1 = 1/2X_1e^{i(\omega_1t+\theta_1)} + cc$, $x_2 = 1/2X_2e^{i(\omega_2t+\theta_2)} + cc$, $\lambda_1 = 1/2\Lambda_1e^{i(\Omega_1t+\tau_1)} + cc$, and $\lambda_2 = 1/2\Lambda_2e^{i(\Omega_2t+\tau_2)} + cc$, where cc is the complex conjugate, these equations can be solved by a first-order approximation and result in the following amplitude and phase equations of each mode:

$$\begin{aligned}\dot{X}_1 &= \mathrm{K}_1\sin(\gamma_1) + \delta_1X_2X_1^2\sin(\gamma_3) - \frac{\Delta\omega_1}{2}X_1\\ \dot{\theta}_1 &= -\mathrm{K}_1\cos(\gamma_1) - \alpha_1X_1^2 - \beta_1X_2^2 - \delta_1X_1X_2\cos(\gamma_3)\\ \dot{X}_2 &= \mathrm{K}_2\sin(\gamma_2) - \delta_2X_1^3\sin(\gamma_3) - \frac{\Delta\omega_2}{2}X_2\\ \dot{\theta}_2 &= -\mathrm{K}_2\cos(\gamma_2) - \alpha_2X_2^2 - \beta_2X_1^2 - \delta_2\frac{X_1^3}{X_2}\cos(\gamma_3).\end{aligned} \tag{2}$$

Here, γ_1 and γ_2 are the phase-shifts of the external forces λ_1 and λ_2 which are fixed by the PLL, while γ_3 is associated with the phase difference between the oscillations of the two modes. For simplification and to provide an intuitive explanation of coupling, we have introduced four new variables: K, α, β, and δ. These variables are further explained in the supplementary material; here a concise explanation is provided. K_1 and K_2 represent the external forcing terms. The next four terms relate to amplitude-frequency dependence: $\alpha_1X_1^2$ and $\alpha_2X_2^2$ are the standard terms causing a shift in frequency due to Duffing nonlinearity, while $\beta_1X_2^2$ and $\beta_2X_1^2$ are terms causing a shift in frequency due to coupling between the two modes. Measured values for these four terms are presented in the supplementary material. Finally, δ_1 and δ_2 are the coupling coefficients which cause the internal resonance and consequently synchronization between the two modes. The terms including δ_1 and δ_2 in the equations, depend on the amplitudes of both modes, resulting in amplitude dependence of the synchronization behavior. For example, $\delta_1X_1X_2\cos(\gamma_3)$ and $8\delta_2\frac{X_1^3}{X_2}\cos(\gamma_3)$, both depend on X_1 and X_2. The coupling term $8\delta_2\frac{X_1^3}{X_2}\cos(\gamma_3)$ decreases as X_2 (the amplitude of the 9θ mode) increases; this fact results in decreased coupling from the 3θ mode to the 9θ mode and consequently the synchronization range decreases. On the other hand, all the coupling terms increase with the amplitude of the 3θ mode (X_1), resulting in an increased synchronization range.

Previous studies have shown that in a single nonlinear oscillator, the synchronization range increases with the oscillator's energy (amplitude squared).[9,10,20] The model in Eq. (2) predicts similar behavior as the energy of the first oscillator (3θ mode) is increased. More importantly, it also predicts the surprising result that increasing the energy of the second oscillator (9θ mode) results in a decrease in the synchronization range. This observation is in contrast with the reported behavior of injection-locked oscillators,[9,10] and mutually synchronized oscillators[20] in which the synchronization range always increases with oscillator amplitude. We have conducted measurements to experimentally prove these predictions. Figure 3 illustrates a 3D plot of the measured synchronization range compared with the numerical solution from the model of Eq. (2) for drive voltages ranging from 450 mV to 750 mV for the 3θ mode and from 15 mV to 55 mV for the 9θ mode. These data illustrate that the synchronization range increases with the energy in the first mode (X_1^2) and has an inverse relationship with the energy in the second mode (X_2^{-2}).

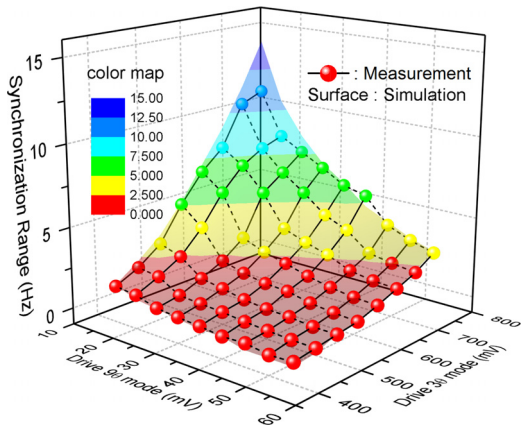

FIG. 3. 3D plot illustrating the measured (spheres) and simulated (surfaces) dependence of the synchronization range on the drive voltages of both oscillators. The synchronization range increases with the 3θ mode oscillator's amplitude and decreases with the 9θ mode oscillator's amplitude.

To further validate the model and understand the synchronization dynamics, we compare the measured behavior of the oscillators in the synchronized state with the behavior predicted by the model. While synchronized, the frequency of the two modes will follow each other. The measured amplitude, phase, and frequency presented in Fig. 4 show the behavior as the tuning voltage is varied at the operating point where the two oscillators are driven at 700 mV (3θ mode) and 35 mV (9θ mode). When synchronized, the oscillator frequency versus tuning voltage deviates from a straight line, an effect which is also predicted by the model, and is different from the behavior of injection-locked oscillators.[9,10,12,39] Looking at the oscillator amplitudes in Fig. 4, this frequency deviation occurs at a point where the bidirectional coupling results in energy transfer between the two modes: X_1 diminishes and X_2 grows. The changing amplitudes in turn affect the frequency through the amplitude-frequency dependence produced by the Duffing nonlinearity, $\alpha_1 X_1^2$ and $\beta_1 X_2^2$. The parameter values needed to reproduce Figs. 3 and 4 are provided in the supplementary material.

In conclusion, we demonstrated synchronization between two oscillators based on two distinct resonance modes of a single resonator. Using a coupled-oscillator model, we showed that this 3:1 subharmonic synchronization originates from cubic, non-dissipative electromechanical coupling. In agreement with the model, the synchronization range for subharmonic frequency entrainment increases with the energy in the subharmonic oscillator and decreases with the energy of the higher frequency oscillator. These results illustrate the previously unexplored dynamics of subharmonic synchronization between two intrinsically coupled modes in a single micromechanical resonator, a phenomenon which may have applications in weak signal detection, mechanical signal processing, and frequency stabilization of micromechanical sensors and timing oscillators.

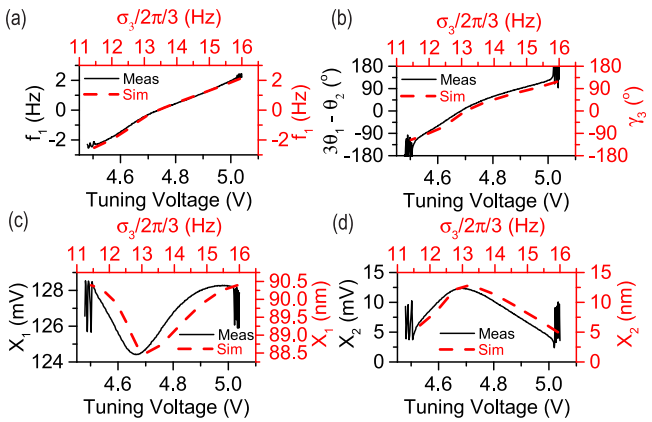

FIG. 4. Synchronization: comparison of the model (red dashed lines) and the measurements (solid black lines): (a) synchronized frequency, (b) synchronized phase, (c) amplitude of the first mode, and (d) amplitude of the second mode. In the figure, $\sigma_3 = \omega_2 - 3\omega_1$ represents the frequency detuning of the two oscillators.

See supplementary material for the model and numerical analysis along with additional measurements of the MDR's characteristics.

The authors thank Professor Thomas Kenny and his research group at Stanford University for device fabrication. This work was funded by Berkeley Sensor and Actuator (BSAC) members and DARPA Grant No. W31P4Q-11-1-0003.

[1]S.-J. Wang, X.-J. Xu, Z.-X. Wu, and Y.-H. Wang, Phys. Rev. E **74**, 041915 (2006).
[2]J. M. Cruz, M. Rivera, and P. Parmananda, Phys. Rev. E **75**, 035201 (2007).
[3]M. Xu, D. A. Tieri, E. C. Fine, J. K. Thompson, and M. J. Holland, Phys. Rev. Lett. **113**, 154101 (2014).
[4]N. Locatelli, A. Hamadeh, F. A. Araujo, A. D. Belanovsky, P. N. Skirdkov, R. Lebrun, V. V. Naletov, K. A. Zvezdin, M. Muñoz, J. Grollier, O. Klein, V. Cros, and G. de Loubens, Sci. Rep. **5**, 17039 (2015).
[5]C. Huygens, *Horologium oscillatorium: sive, De motu pendulorum ad horologia aptato demostrationes geometricae* (F. Muguet, 1673).
[6]A. Pikovsky, M. Rosenblum, and J. Kurths, *Synchronization: A Universal Concept in Nonlinear Sciences* (Cambridge University Press, 2003).
[7]R. Adler, Proc. IRE **34**, 351 (1946).
[8]R. D. Huntoon and A. Weiss, Proc. IRE **35**, 1415 (1947).
[9]D. Antonio, D. A. Czaplewski, J. R. Guest, D. López, S. I. Arroyo, and D. H. Zanette, Phys. Rev. Lett. **114**, 034103 (2015).
[10]M. Defoort, P. Taheri-Tehrani, S. H. Nitzan, and D. A. Horsley, ASME. J. Vib. Acoust. **139**(4), 040906–040906-7 (2017).
[11]M. Zalalutdinov, K. L. Aubin, M. Pandey, A. T. Zehnder, R. H. Rand, H. G. Craighead, and J. M. Parpia, Appl. Phys. Lett. **83**, 3281 (2003).
[12]S. Urazhdin, P. Tabor, V. Tiberkevich, and A. Slavin, Phys. Rev. Lett. **105**, 104101 (2010).
[13]M. Belhaq and A. Fahsi, Ann. Solid Struct. Mech. **4**, 15 (2012).
[14]J. Simonet, M. Warden, and E. Brun, Phys. Rev. E **50**, 3383 (1994).
[15]M. G. Rosenblum, A. S. Pikovsky, and J. Kurths, Phys. Rev. Lett. **76**, 1804 (1996).
[16]J. Lü, T. Zhou, and S. Zhang, Chaos, Solitons Fractals **14**, 529 (2002).
[17]M. H. Matheny, M. Grau, L. G. Villanueva, R. B. Karabalin, M. C. Cross, and M. L. Roukes, Phys. Rev. Lett. **112**, 014101 (2014).
[18]H. G. Schuster and P. Wagner, Prog. Theor. Phys. **81**, 939 (1989).
[19]J. Y. Chen, K. W. Wong, and J. W. Shuai, Chaos **12**, 100 (2002).
[20]D. K. Agrawal, J. Woodhouse, and A. A. Seshia, J. Appl. Phys. **115**, 164904 (2014).
[21]O. Shoshani and S. W. Shaw, IEEE Trans. Circuits Syst. I **63**, 1 (2016).
[22]D. K. Agrawal, J. Woodhouse, and A. A. Seshia, Phys. Rev. Lett. **111**, 084101 (2013).
[23]M. Bagheri, M. Poot, L. Fan, F. Marquardt, and H. X. Tang, Phys. Rev. Lett. **111**, 213902 (2013).
[24]M. Zhang, G. S. Wiederhecker, S. Manipatruni, A. Barnard, P. McEuen, and M. Lipson, Phys. Rev. Lett. **109**, 233906 (2012).
[25]M. Nakajima, D. F. Wang, T. Ikehara, T. Itob, and R. Maeda, in *Symposium on Design, Test, Integration and Packaging of MEMS/MOEMS (DTIP)* (2013), pp. 1–4.

[26]M. Nakajima, D. F. Wang, T. Ikehara, T. Itoh, and R. Maeda, in *Symposium on Design, Test, Integration and Packaging of MEMS/MOEMS* (2012), pp. 230–233.
[27]D. Antonio, D. H. Zanette, and D. López, Nat. Commun. **3**, 806 (2012).
[28]C. H. Ahn, E. J. Ng, V. A. Hong, Y. Yang, B. J. Lee, I. Flader, and T. W. Kenny, J. Microelectromech. Syst. **24**, 343 (2015).
[29]Y. Yang, E. J. Ng, Y. Chen, I. B. Flader, and T. W. Kenny, J. Microelectromech. Syst. **25**, 489 (2016).
[30]M. Ignatov, M. Hansen, M. Ziegler, and H. Kohlstedt, Appl. Phys. Lett. **108**, 084105 (2016).
[31]M. Pandey, R. H. Rand, and A. T. Zehnder, Nonlinear Dyn. **54**, 3 (2008).
[32]P. Taheri-Tehrani, M. Defoort, and D. Horsley, J. Micromech. Microeng. **27**, 075015 (2017).
[33]N. Kacem, S. Hentz, D. Pinto, B. Reig, and V. Nguyen, Nanotechnology **20**, 275501 (2009).
[34]S. Nitzan, T. H. Su, C. Ahn, E. Ng, V. Hong, Y. Yang, T. Kenny, and D. A. Horsley, in *IEEE 27th International Conference on Micro Electro Mechanical Systems (MEMS)* (2014), pp. 749–752.
[35]B. J. Gallacher, J. Hedley, J. S. Burdess, A. J. Harris, A. Rickard, and D. O. King, J. Microelectromech. Syst. **14**, 221 (2005).
[36]P. M. Polunin and S. W. Shaw, Int. J. Non-Linear Mech. **94**, 300–308 (2017).
[37]A. H. Nayfeh and D. T. Mook, *Nonlinear Oscillations* (John Wiley & Sons, 2008).
[38]H. Dai, X. Wang, M. Schnoor, and S. N. Atluri, Commun. Nonlinear Sci. Numer. Simul. **49**, 176 (2017).
[39]M. Pandey, K. Aubin, M. Zalalutdinov, R. B. Reichenbach, A. T. Zehnder, R. H. Rand, and H. G. Craighead, J. Microelectromech. Syst. **15**, 1546 (2006).